Science Bulletin 71 (2026) 259–263

Contents lists available at ScienceDirect

Science Bulletin

journal homepage: www.elsevier.com/locate/scib

Short Communication

Precision regulation of flexibility of metal-peptide network membranes towards high-efficiency CO_2 separation

Huijie Wang [a,1], Haiying Yan [a,1], Jiahui Yan [b], Yi Liu [b,*], Chen Wang [a,*]

[a] State Key Laboratory of Microbial Technology, Jiangsu Collaborative Innovation Center of Biomedical Functional Materials, Jiangsu Key Laboratory of New Power Batteries, School of Chemistry and Materials Science, Nanjing Normal University, Nanjing 210023, China
[b] State Key Laboratory of Fine Chemicals, Frontiers Science Center for Smart Materials, School of Chemical Engineering, Dalian University of Technology, Dalian 116024, China

ARTICLE INFO

Article history:
Received 28 June 2025
Received in revised form 28 October 2025
Accepted 24 November 2025
Available online 1 December 2025

The increasing atmospheric concentration of carbon dioxide (CO_2) urgently demands advanced carbon capture solutions. Post-combustion carbon capture from flue gas (primarily CO_2 and N_2) is pivotal for achieving carbon neutrality, yet the similar kinetic diameters of CO_2 and N_2 make accurate separation difficult using traditional techniques [1,2]. Nanofluidic membranes stand out as advanced technology for gas separation, given their low energy consumption, operation simplicity, compact design, and scalability [3]. Among them, rigid membranes, which have gained significant attention, can distinguish guest molecules by affinity or size differences [4]. However, precise pore and shape control is needed for achieving size-selective exclusion, but slow kinetics and low permeability in narrow pores limit their applications [5]. Notably, flexible membranes that exhibit pressure, temperature, and size/shape adaptability, enable high-efficiency gas separation via guest-dependent threshold pressures [6,7], thus eliminating the need for precise pore size control through a "switch-like" separation mechanism [8,9].

Metal-peptide network (MPN), which can be assembled using peptides and metal ions, represents one of the most captivating metal–organic coordination frameworks, owing to its unique and intricate structure [10]. The network capitalizes on peptides, fundamental biomolecules that are ubiquitous in biological systems, as superior natural ligands for constructing a flexible porous framework. The inherent polar functional groups in peptides, including amides, carboxylates, and amines, engage in strong quadrupole-dipole interactions with CO_2 molecules [11], presenting remarkable potential for preferential CO_2 adsorption. In addition, the structural versatility of MPN can be engineered by pairing different amino acids, allowing precise tuning of framework-gas molecule interactions [12]. However, current research on amino acids or peptides in gas separation mainly focuses on post-synthetic modification, which often has low efficiency and affects membrane reliability and stability [2]. Therefore, developing precise and controllable MPN membrane fabrication methods is crucial for practical gas separation applications.

In this study, pressure-responsive MPN membranes with tunable flexibility were fabricated from Zn^{2+}-coordinated Gly-Gly (GG), Gly-Ala (GA), and Gly-Ser (GS)dipeptides grown on anodized aluminum oxide (AAO) substrates for efficient CO_2/N_2 separation (Fig. 1a). Since CO_2 strongly interacts with polar groups in dipeptides (amides, carboxylic acids, and amines) through quadrupole-dipole interactions and overcomes framework deformation energy [11], a closed-to-open pore transition is triggered in MPN membranes, enabling preferential CO_2 permeation while blocking N_2. Compared to GG-MPN/AAO, in GA-MPN/AAO, methyl groups increase steric hindrance and rigidity, raising gate-opening pressure to suppress CO_2/N_2 co-permeation. Methyl groups in GA-MPN/AAO also fine-tune the pore aperture, boosting CO_2/N_2 selectivity. In contrast, the more rigid GS-MPN/AAO (with hydroxymethyl) retained closed pores at 10 bar (1 bar = 10^5 Pa) CO_2, reducing CO_2/N_2 selectivity. Therefore, GA-MPN/AAO exhibited superior performance among three MPN membranes, achieving CO_2/N_2 selectivity of 40.8 and CO_2 permeance of 1553.3 GPU at 298 K, which well surpasses the Robeson upper bound, thereby offering a new protocol for fabricating next-generation pressure-responsive membranes.

Zinc (II) nitrate and glycyl-X were reacted in a methanol solution containing 1 mol L^{-1} NaOH to synthesize MPN (defined as GX-MPN). These networks were derived from three different dipeptides: GG, GA, and GS (Fig. S1 online) [11,12]. Herein X denotes

* Corresponding authors.
E-mail addresses: diligenliu@dlut.edu.cn (Y. Liu), wangchen@njnu.edu.cn (C. Wang).
[1] These authors contributed equally to this work.

https://doi.org/10.1016/j.scib.2025.11.058

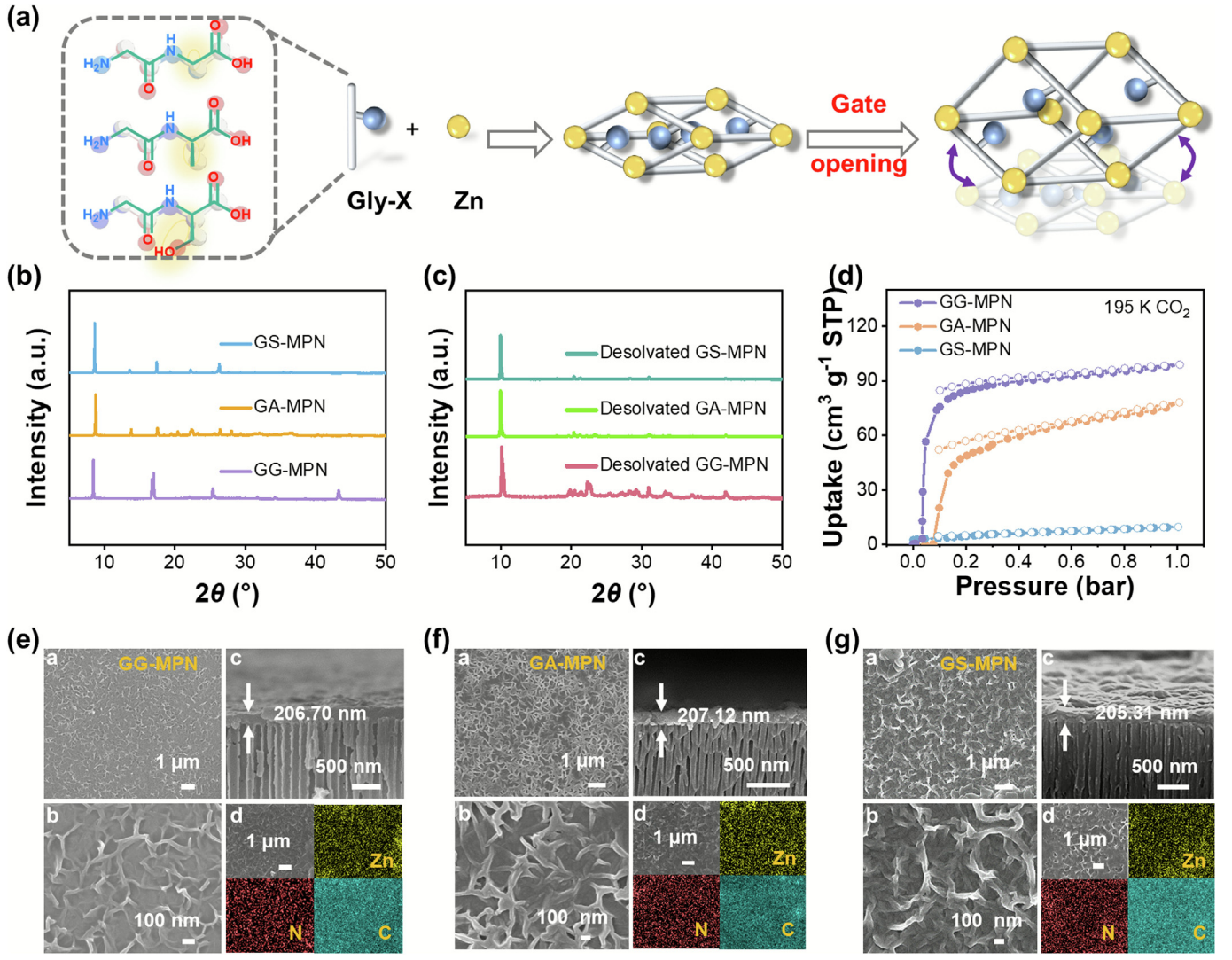

Fig. 1. Preparation and characterization of MPN membranes with different side chains of dipeptide. (a) GX-MPN was synthesized using dipeptide linkers with different side chains (Gly-Gly, Gly-Ala, and Gly-Ser), featuring an open-pore mechanism. (b) PXRD patterns of GG-MPN, GA-MPN, and GS-MPN. (c) PXRD patterns of GG-MPN, GA-MPN, and GS-MPN after solvent removal. (d) The CO_2 adsorption isotherms at 195 K of GG-MPN, GA-MPN, and GS-MPN. (e–g) SEM images of (e) GG-MPN/AAO, (f) GA-MPN/AAO, and (g) GS-MPN/AAO (a, b: the top; c: cross section; d: EDX elemental mappings of MPN).

chemically modified residues with different functional groups at the alpha carbon position of the C-terminal, including GG (no functional groups, the simplest oligopeptide [13]), GA (one methyl group), and GS (one methyl and one hydroxyl group) (Fig. 1a). Each dipeptide coordinates two Zn^{2+} metal ions through the N-terminal amine of Gly and the C-terminal carboxylate of residue X, forming a bridging coordination network and indicating the formation of one-dimensional open lozenge-shaped channels (Fig. S1 online). Fourier transform infrared (FTIR) spectra demonstrated the formation of GG-MPN, GA-MPN, and GS-MPN, with the detection of –C=O (1613–1658 cm^{-1}), –C–N (1087–1110 cm^{-1}), –NH (3274–3292 cm^{-1}), and –OH (2941–2978 cm^{-1}) (Fig. S2 online). Besides, powder X-ray diffraction (PXRD) revealed that the above materials were isostructural analogues, as evidenced with simulated PXRD patterns (Fig. 1b and Fig. S3 online). Interestingly, after solvent removal, XRD peaks of GG-MPN, GA-MPN, and GS-MPN shifted toward higher angles (approximately from 2θ = 8.6° to 10.0°) (Fig. 1c). This shift indicates a unit cell contraction, a phenomenon well-documented in flexible porous frameworks, where the removal of guest molecules triggers a reversible phase transition from a large-pore (open) to a narrow-pore (closed) state [12]. This confirms the stimuli-responsive nature of our MPNs.

To demonstrate the structural properties, CO_2 adsorption isotherms of GX-MPN were measured at 195 K (Fig. 1d). The CO_2 adsorption isotherms of GA-MPN and GG-MPN both exhibited step-shaped characteristics, with GG-MPN showing a sharp increase in CO_2 uptake at 0.03 bar and GA-MPN displaying a similar increase at 0.07 bar. In contrast, GS-MPN did not exhibit any sharp increase in CO_2 uptake (Fig. 1d). The delayed increase in CO_2 uptake for GA-MPN can be attributed to the appropriate rigidity introduced by the methyl side chain of GA. The CO_2 adsorption isotherm of GS-MPN lacked step-shaped characteristics, owing to the excessive rigidity imparted by the hydroxymethyl side chains, which precluded pore opening under the specific conditions [12]. Conversely, activated GG-MPN, GA-MPN, and GS-MPN exhibited negligible N_2 uptake at 77 K adsorption isotherms (Figs. S4–S6 online), indicating that non-polar N_2 (Table S1 online) failed to induce pore opening for guest accommodation [11]. Finally, TGA was conducted to assess the thermal stability of GG-MPN, GA-MPN, and GS-MPN. Our results indicate that all three compounds

exhibit thermal stability up to 270 °C under N_2 conditions (Fig. S7 online), which is essential for maintaining structural integrity during gas separation processes.

Subsequently, dipeptide-based MPN was *in situ* synthesized on a fabricated porous AAO substrate (Fig. S8 online) through the anodization oxidation technique [14]. Amino-functionalized AAO reacts with the carboxyl group in dipeptide ligands (GG, GA, or GS) to form the initial layer of MPN membrane. The absorbance peaks of amide I (~1650 cm^{-1}) and amide II (~1060 cm^{-1}) in FT-IR spectroscopy correspond to C=O and C–N stretching, confirming the bonding between carboxylic groups in the MPN and amine groups in AAO (Fig. S9 online), and the highly hydrophilic nature of the MPN membranes was further verified by water contact angle measurements (Fig. S10 online). Then, diverse MPN membranes were fabricated on AAO substrates via *in situ* growth at 85°C for 18 h using different dipeptide ligands (GG, GA, or GS). X-ray photoelectron spectroscopy (XPS) confirmed successful introduction of amino groups and MPN on AAO via Si 2p (amino-functionalized AAO) and Zn 2p (MPN/AAO) peaks (Fig. S11 online), with no signals on bare AAO. Scanning electron microscope (SEM) was further employed to study the morphology of MPN membranes. SEM analysis showed that the MPN membrane uniformly coated the AAO substrate (50 nm channels, Fig. S12 online) without cracks, while the lower surface retained ordered channels (Fig. S13 online). The energy dispersive X-ray spectroscopy (EDX) image showed uniform C, N, and Zn distribution on the membrane surface. Cross-section imaging revealed a 200 nm-thick MPN layer tightly adhered to the AAO (Fig. 1e–g). MPN layer thickness depended on reaction time: discontinuous layers formed within 12 h (Figs. S14-S19 online), complete coverage occurred at 18 h (Fig. 1e–g), and defect-free membranes resulted at 24 h (Figs. S20–S22 online). However, a 24 h reaction produced a thicker (~500 nm) layer with undesired surface protrusions (Figs. S20–S22 online). Considering that a larger thickness would lead to reduced gas permeability, the MPN layer with 18 h reaction time was adopted in the following experiments (Fig. S23 online). Atomic-force-microscopy (AFM) analysis further confirmed the homogeneous surface morphology of the MPN membrane (Fig. S24 online).

Simultaneously, the adsorption isotherms of pure CO_2 and N_2 on GG-MPN, GA-MPN, and GS-MPN were evaluated at temperatures of 298 K, with the maximum pressure reaching 10 bar (Fig. 2a and Figs. S25, S26 online). At low pressures (< 2.4 bar),

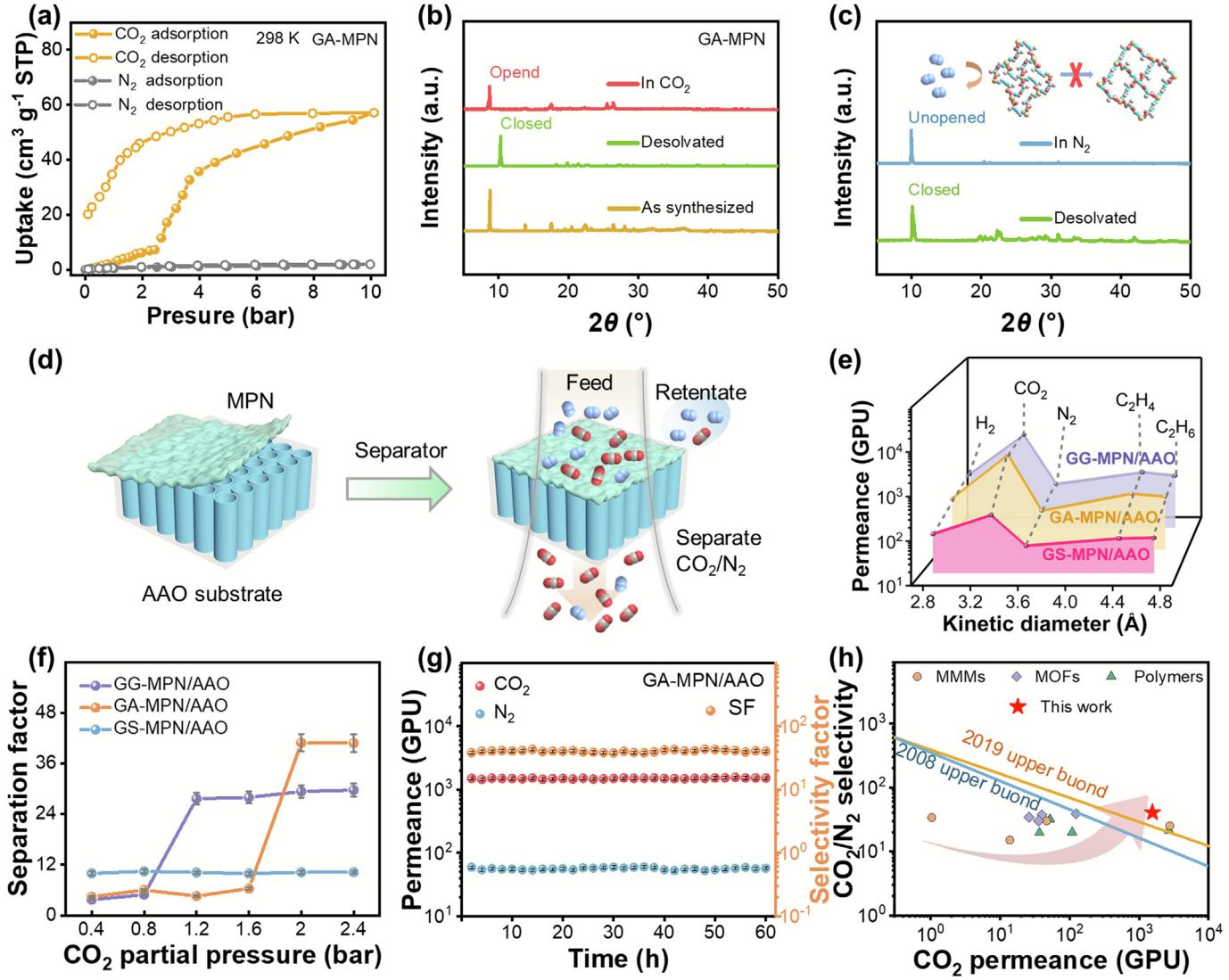

Fig. 2. Gas separation performance and separation mechanism of the GX-MPN. (a) Single-component adsorption isotherms of CO_2 and N_2 at 298 K of GA-MPN. (b) PXRD patterns of GA-MPN in closed-pore and open-pore states. (c) PXRD patterns of GA-MPN under N_2 atmosphere. (d) Schematic diagram of GX-MPN/AAO membrane separation of CO_2 and N_2. (e) The single component gas permeability of H_2, CO_2, N_2, C_2H_4, and C_2H_6 for three types of GX-MPN/AAO. (f) Selectivity comparison of GG-MPN/AAO, GA-MPN/AAO, and GS-MPN/AAO with different CO_2 partial pressure at 298 K. (g) Long-term separation stability of GA-MPN/AAO. All of the tests were conducted at 298 K and 2.5 bar. (h) The performance comparison of CO_2/N_2 separation between the prepared membranes in this work with other reported membranes in the literature.

GA-MPN was nonporous to CO_2 adsorption at 298 K. Nonetheless, phase transformation to the open pore structure occurred at 2.4 bar (Fig. 2a). The CO_2 adsorption capacity at 298 K was determined to be 57.13 $cm^3\ g^{-1}$. Conversely, the adsorption of N_2 for GA-MPN was negligible at 298 K with an adsorption capacity of 2.02 $cm^3\ g^{-1}$. Similarly, GG-MPN exhibited negligible CO_2 adsorption below 1.4 bar (Fig. S25 online), but underwent a pronounced pressure-activated adsorption transition at 1.4 bar. The CO_2 uptake then rose sharply with increasing pressure, reaching an adsorption capacity of 67.2 $cm^3\ g^{-1}$ at 10 bar. Notably, GG-MPN displayed extremely low N_2 adsorption (< 3.0 $cm^3\ g^{-1}$) under the same conditions, with no gate-opening observed, which was consistent with the behavior of GA-MPN. In contrast, GS-MPN exhibited CO_2 adsorption at 298 K without a distinct gating phenomenon, only achieving an uptake of 9.5 $cm^3\ g^{-1}$ (Fig. S26 online). It also showed very low N_2 adsorption (< 1.9 $cm^3\ g^{-1}$) with no pressure-responsive behavior. These findings demonstrate that the adsorption gating pressure of these materials can be precisely controlled by dipeptide side chain modulation, providing an effective means for gas adsorption and separation processes. To further gain insights into gas-induced structural transformation, XRD patterns of GA-MPN were collected under CO_2 atmosphere at 298 K (Fig. 2b). Experimental results indicated that the characteristic peak shifted from 2θ = 10.0° to 8.7° under CO_2 exposure. This shift was attributed to the opening of the pore channels upon CO_2 adsorption, which facilitated CO_2 molecule entry into the framework and confirmed the presence of host–guest interactions [11]. In contrast, the peak position did not change in the presence of N_2 (Fig. 2c), demonstrating that the interaction between N_2 and MPN framework is negligible.

Finally, CO_2/N_2 separation performance of the MPN membrane was evaluated using a Wicke-Kallenbach apparatus [1] (Fig. 2d and Figs. S27, S28 online). Single-gas permeation results showed significant cut-off between CO_2 and N_2 for GG-MPN/AAO, GA-MPN/AAO, and GS-MPN/AAO (Fig. 2e). GA-MPN/AAO achieved CO_2 permeance of 1789.6 GPU and CO_2/N_2 selectivity of 32.1, while GG-MPN/AAO and GS-MPN/AAO exhibited selectivity of 24.4 and 7.6, respectively, all exceeding their Knudsen selectivity (Figs. S29–S31 online). The CO_2/N_2 separation performance of GG-MPN/AAO, GA-MPN/AAO, and GS-MPN/AAO was evaluated using binary feeds with different CO_2 partial pressures (Fig. 2f and Fig. S32 online). As depicted in Fig. 2f, GA-MPN/AAO showed a distinct gas cut-off capability as CO_2 partial pressure increased from 0.1 to 2.5 bar, with a gate-opening pressure at 2 bar. This was accompanied by an increase in CO_2 permeability from 177.1 to 1553.3 GPU and a selectivity rise from 6.3 to 40.8. In comparison, GG-MPN/AAO exhibited a sharp increase in CO_2 permeability from 307.6 to 1751.3 GPU at 1.2 bar, yet its selectivity was relatively low, increasing only from 4.9 to 29.7. GS-MPN/AAO exhibited no pore opening within the 2.5 bar range and had a low CO_2 permeability of around 200 GPU. The selectivity differences are further illustrated in Fig. 2f. The variation in gate-opening pressure originates from the differences in dipeptide side chains. Specifically, the methyl group in GA-MPN/AAO introduces greater steric hindrance and framework rigidity than that in GG-MPN/AAO [15]. This increased rigidity, which in turn raises the gate-opening pressure, effectively suppresses N_2 co-permeation. This group also reduces pore size, boosting CO_2/N_2 selectivity. In contrast, GS-MPN/AAO shows no pore-opening behavior, leading to lower selectivity. The stability of CO_2/N_2 separation was tested further (Fig. 2g). After 60 h, the GA-MPN/AAO membrane showed excellent durability, with negligible decreases in CO_2 permeability and selectivity, which was corroborated by unchanged post-test SEM and XRD analyses (Figs. S33, S34 online). Significantly, the GA-MPN/AAO membrane maintained stable CO_2/N_2 separation performance under demanding conditions, showing only moderate and reversible changes in permeability and selectivity during a 10 h test at 100 °C and under high humidity (Figs. S35, S36 online). Furthermore, the performance of GA-MPN/AAO surpassed the 2008 and 2019 upper bound for CO_2/N_2 separation and the reported outcomes of most studies (refer to Fig. 2h and Table S2 online). These results demonstrate that the framework flexibility can be effectively tuned by altering the side-chain functional groups of the dipeptides, thereby enhancing overall membrane performance.

In summary, this work demonstrates the novelty of precise regulation of CO_2 gate-opening pressure in metal-peptide network membranes through dipeptide side-chain engineering. The GA-MPN membrane, with optimal rigidity imparted by a methyl group, achieves superior CO_2/N_2 separation performance (selectivity of 40.8), well surpassing the Robeson upper bound. This side-chain mediated flexibility tuning strategy presents a new paradigm for developing adaptive membranes. Meanwhile, a key limitation is the performance attenuation under simulated flue gas conditions, which highlights the challenge of maintaining high selectivity in complex industrial environments. Addressing the stability in realistic streams and the scalability of membrane fabrication remain pivotal for future practical applications.

Conflict of interest

The authors declare that they have no conflict of interest.

Acknowledgments

This work was supported by the National Natural Science Foundation of China (22274076 and 22304084) and the Primary Research & Development Plan of Jiangsu Province (BE2022793).

Author contributions

Yi Liu, Chen Wang, Huijie Wang, and Haiying Yan conceived and supervised the project. Huijie Wang and Haiying Yan performed experiments. Yi Liu, Chen Wang, Huijie Wang, and Jiahui Yan linked experiments and analysis. All the authors discussed and wrote the manuscript.

Appendix A. Supplementary material

Supplementary data to this article can be found online at https://doi.org/10.1016/j.scib.2025.11.058.

References

[1] Sun Y, Yan J, Jiang J, et al. Hierarchical defect-rich UiO-66 membrane towards superior flue gas and butane isomer separations. Sci Bull 2024;69:2174–8.
[2] Chen Z, Zhang P, Wu H, et al. Incorporating amino acids functionalized graphene oxide nanosheets into Pebax membranes for CO_2 separation. Sep Purif Technol 2022;288:120682.
[3] Yang K, Hu S, Ban Y, et al. ZIF-L membrane with a membrane-interlocked-support composite architecture for H_2/CO_2 separation. Sci Bull 2021;66:1869–76.
[4] Li W, Su P, Tang H, et al. Hetero-polycrystalline membranes with narrow and rigid pores for molecular sieving. Small 2022;19:2205542.
[5] Zhou S, Shekhah O, Ramírez A, et al. Asymmetric pore windows in MOF membranes for natural gas valorization. Nature 2022;606:706–12.
[6] Dong J, Wee V, Zhao D. Stimuli-responsive metal–organic frameworks enabled by intrinsic molecular motion. Nat Mater 2022;21:1334–40.
[7] Ying Y, Zhang Z, Peh SB, et al. Pressure-responsive two-dimensional metal-organic framework composite membranes for CO_2 separation. Angew Chem Int Ed 2021;60:11318–25.
[8] Zhang Z, Zhu H, Jin H, et al. Restricting linker rotation in nanocages of ZIF-8 membranes using crown ether "molecular locks" for enhanced propylene/propane separation. Angew Chem Int Ed 2024;64:e202415023.
[9] Tian X, Cao L, Zhang K, et al. Molecular weaving towards flexible covalent organic framework membranes for efficient gas separations. Angew Chem Int Ed 2024;64:e202416864.

[10] Kim J, Hong J, Park MJ, et al. Tailoring enantiomeric chiral channels in metal-peptide networks: a novel foldamer-based approach for host-guest interactions. Adv Mater 2023;35:2305753.
[11] Rabone J, Yue Y-F, Chong SY, et al. An adaptable peptide-based porous material. Science 2010;329:1053–7.
[12] Martí-Gastaldo C, Antypov D, Warren JE, et al. Side-chain control of porosity closure in single- and multiple-peptide-based porous materials by cooperative folding. Nat Chem 2014;6:343–51.
[13] Cabezas C, Varela M, Alonso JL. The structure of the elusive simplest dipeptide gly-gly. Angew Chem Int Ed 2017;56:6420–5.
[14] Wang H, Zhang Y, Wang J, et al. *In situ* synthesized HOF ion rectification membrane with ultrahigh permselectivity for nanofluidic osmotic energy harvesting. Adv Funct Mater 2024;35:2412477.
[15] Yan Y, Carrington EJ, Pétuya R, et al. Amino acid residues determine the response of flexible metal-organic frameworks to guests. J Am Chem Soc 2020;142:14903–13.